Irrigation Signals Detected from SMAP Soil Moisture Retrievals

Patricia M. Lawston[1,2], Joseph A. Santanello, Jr.[2], Sujay V. Kumar[2]

[1]Earth System Science Interdisciplinary Center, University of Maryland, College Park, Maryland, USA.

[2]Hydrological Sciences Laboratory, NASA Goddard Space Flight Center, Greenbelt, Maryland, USA.

Corresponding author: Patricia Lawston (patricia.m.lawston@nasa.gov)

Key Points:

- To date, irrigation detection from passive microwave satellites has proven difficult even over well-known, expansive regions of agriculture
- The new, enhanced soil moisture product from the Soil Moisture Active Passive satellite can detect irrigation signals in three regions
- Satellite detection of irrigation increases our ability to understand, monitor, and predict human impacts on the water cycle.

Abstract

Irrigation can influence weather and climate, but the magnitude, timing, and spatial extent of irrigation are poorly represented in models, as are the resulting impacts of irrigation on the coupled land-atmosphere system. One way to improve irrigation representation in models is to assimilate soil moisture observations that reflect an irrigation signal to improve model states. Satellite remote sensing is a promising avenue for obtaining these needed observations on a routine basis, but to date, irrigation detection in passive microwave satellites has proven difficult. In this study, results show that the new Enhanced soil moisture product from the Soil Moisture Active Passive (SMAP) satellite is able to capture irrigation signals over three semi-arid regions in the western United States. This marks an advancement in earth-observing satellite skill and the ability to monitor human impacts on the water cycle.

Plain Language Summary

When farmers use irrigation over large areas, it can make the air cooler and more humid; sometimes even changing how clouds form and where rain falls. For this reason, it's important to know where and when irrigation is used, how wet the soil becomes, and how long it stays artificially wet. This information is critical for improving weather models, and therefore forecasts, in the food baskets of the world. However, until now it has been difficult to find accurate and consistent irrigation practice information over time and for large areas. In this paper, we show that a NASA satellite which measures soil moisture routinely across the globe is able to detect wet soil resulting from irrigation in naturally dry environments. This marks an advancement in earth-observing satellite skill and improves our ability to monitor and predict human impacts on the water cycle.

1 Introduction

Irrigation is required to meet the world's food demands, but also drastically alters the water cycle. By increasing soil moisture (SM), irrigation repartitions the surface energy balance, increasing evaporation and decreasing sensible heat flux and temperature (Kanamaru & Kanamitsu, 2008; Bonfils & Lobell, 2007). The altered energy balance can be significant enough to influence clouds and precipitation through land-atmosphere interactions driven by planetary boundary layer feedbacks (Kueppers & Snyder, 2011; Qian et al., 2013; Lawston et al., 2015). Thus, irrigation has shown the potential to impact the atmosphere from local to climate scales and is increasingly recognized as an important process for representation in weather and climate models (Sorooshian et al. 2011; Alter et al. 2015; Puma and Cook, 2010*;* among others).

Two main avenues exist for incorporating irrigation into weather models: 1) irrigation parameterizations, and 2) data assimilation (DA) of surface observations. Irrigation modules have grown in complexity (Ozdogan et al. 2010; Evans and Zaitchik, 2010; Leng et al. 2014; Pokhrel et al., 2016), but consistent irrigation practice and SM data are needed globally to evaluate and improve these parameterizations (Lawston et al., 2017). DA avoids the need for assumptions of human practices, but the SM observations must be skillful enough to represent the irrigation signals (Kumar et al. 2015). Thus, to fully leverage either of these avenues requires SM observations with high enough spatial and temporal resolution to distinguish differences between irrigated and non-irrigated areas.

Satellite remote sensing of SM is a natural choice to address this need, but to date it has been difficult to detect irrigation in passive SM retrievals. Kumar et al. (2015) showed the Advanced Scatterometer (ASCAT), the Advanced Microwave Scanning Radiometer 2 (AMSR2), and the Soil Moisture Ocean Salinity (SMOS) were unable to identify seasonal features of irrigation in the California Central Valley, and showed limited skill at best in Nebraska. The most recent SM mission, NASA's Soil Moisture Active Passive (SMAP), has shown improved information content as compared to previous SM satellites (Kumar et al. 2017), raising interest in whether SMAP also shows improvement in irrigation detection. In this study, we explore the utility of SMAP SM retrievals for identifying irrigated regions and timing. While other satellite-based irrigation detection methods exist (e.g., optical/thermal infrared, Thenkabail et al., 2009), the ~two-day return time of SMAP and the ability to directly monitor SM conditions could offer a distinct and advantageous approach for obtaining routine irrigation information.

2 Data and Methods

2.1 Data

The SMAP satellite, launched in January 2015, contains a L-band passive microwave radiometer and uses a single channel retrieval algorithm to provide near surface (i.e., 0-5cm) SM globally, every 1-3 days at 36 km resolution (Entekhabi et al., 2010). SMAP validation studies show that the accuracy of the SM products meets mission requirements (<4%; Colliander et al., 2017) and that SMAP can be used to assess hydrologic processes, such as SM drydowns (Shellito et al., 2016; McColl et al., 2017). The SMAP Level 3 Enhanced SM dataset, used in this study, exploits the oversampling of the antenna overpasses to enhance the spatial resolution of the SM retrievals, posted on a 9 km grid (O'Neill et al., 2016). The analysis focuses on 2016, the only full year available of the Enhanced dataset.

As SM is likely to deviate from the precipitation signal during irrigation periods, Stage IV quantitative precipitation estimates from the National Center for Environmental Prediction are analyzed together with SM. These estimates are derived from radar and rain gauges and gridded at 4 km resolution. Additional in-situ precipitation data are used from the California Irrigation Management Information System (CIMIS) and the Community Collaborative Rain, Hail, & Snow (CoCoRaHS) network.

Datasets used to infer local agricultural practices are the Crop Progress and Condition Bulletins from United States Department of Agriculture National Agricultural Statistical Service (USDA NASS, 2016) and the Terra True Color Reflectance image dataset from Moderate Resolution Imaging Spectroradiometer (MODIS). The crop bulletins are useful for assessing planting, harvest, and growth conditions, while the MODIS images offer a detailed view of the changing landscape that can corroborate the timing of crop growth and harvest.

2.2 Methods

The aforementioned datasets are analyzed for three regions in the western United States, known to contain a range of irrigated agriculture (Figure 1). The Sacramento Valley in northern California, the San Luis Valley in southern Colorado, and the Columbia River Valley in southeastern Washington are semi-arid regions and receive the majority of their precipitation in winter. Thus, warm season irrigation is required to cultivate crops, creating a stark contrast in

vegetation, and presumably SM, between the irrigated agriculture and surrounding precipitation-deficient area. These three regions are chosen to explore the outcome of differing irrigation practices, spatial extent, and other complicating factors on the detection from SMAP.

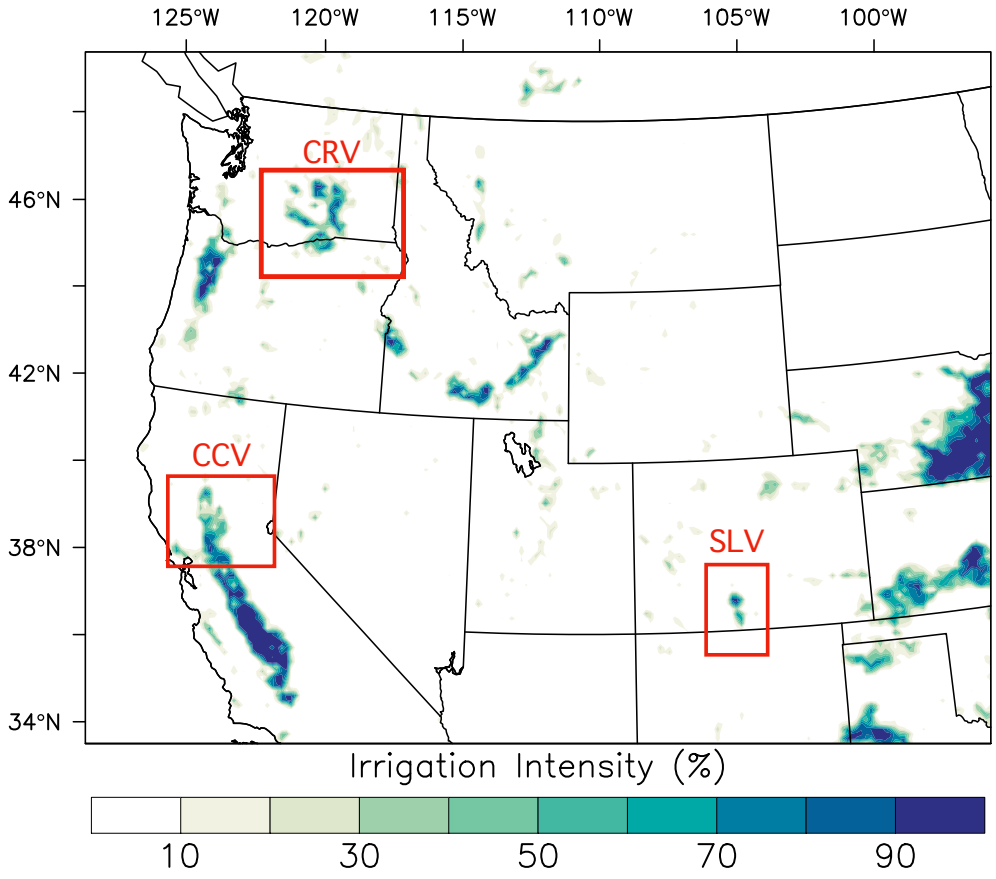

Figure 1. Three case study regions: the Sacramento Valley (CCV), California; San Luis Valley (SLV), Colorado; Columbia River Valley (CRV), Washington, overlaid on percent of areas equipped for irrigation (Salmon et al. 2015).

For each region, the sensitivity of SMAP SM retrievals to irrigation is analyzed as follows: 1) spatially for selected dates during and outside of the growing season, 2) temporally at irrigated and non-irrigated points over a full year, and 3) by using a regional, time-integrated and normalized metric of SM and precipitation to assess the bulk signal in mid-summer. This third metric is calculated by summing the SMAP SM retrievals over June and July 2016 and then normalizing by the minimum and maximum for each study area and time period (hereafter 'integrated SM'). Only days in which SMAP provides full coverage of each study area are used. The same calculations are completed using the Stage IV gridded precipitation to obtain the time-integrated, normalized precipitation (hereafter, 'integrated rainfall'). The resulting maps allow for quick identification of the wettest areas in terms of SM and those that received the greatest rainfall in each region. Assuming relatively similar surface and soil properties and topography, consistently high SM corresponding with relatively low precipitation over the growing season can be used as an indicator of irrigation. All three analyses were completed for each study area,

but for brevity, only the complete set of analyses is shown for the first case study. The remaining analyses are included in the supplement.

3 Results

3.1 Sacramento Valley

The Sacramento Valley, in the northern California Central Valley (CCV), produces 95% of California's rice (CA Rice, 2017). Each year, the fields are flooded and aerially seeded in late April through early May. The water level is sustained throughout the season and then drained shortly before maturity, typically in August. Harvest begins in September and concludes in November (CA Rice, 2017).

Figure 2 shows the significant change in landscape appearance from Terra imagery on February 1, during the wet season, as compared to July 10, during the dry season. The greenness over the region present in February turns brown by July, with the exception of only the irrigated rice and higher elevation forests. SMAP SM retrievals identify these contrasts as February is uniformly wet (> 0.30 cm^3/cm^3) and July is dry except for the irrigated valley and forest, which show much higher SM. This figure implies that SMAP is realistically sensing seasonal SM characteristics and that SM is elevated in the irrigated valley.

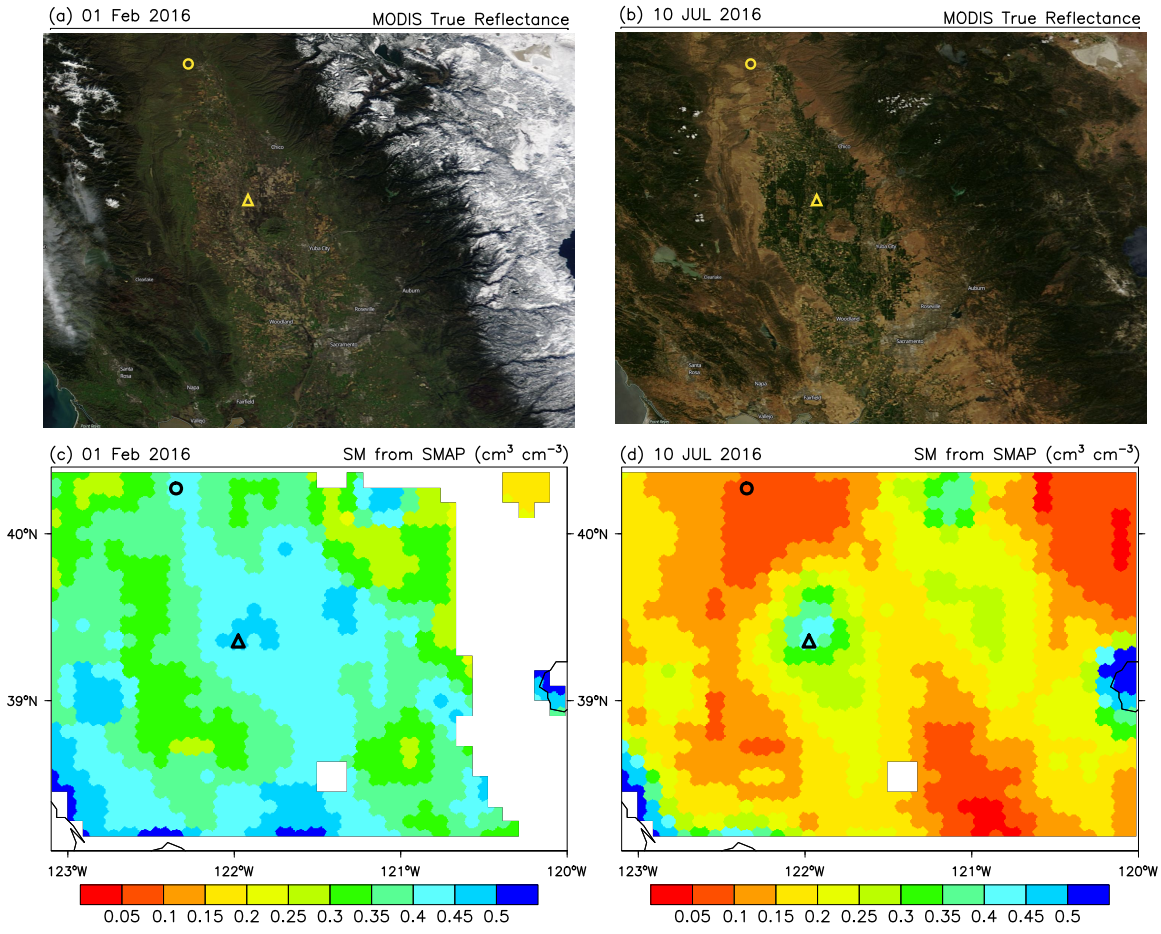

Figure 2. MODIS Terra true color reflectance for (a) February 1, 2016 and (b) July 10, 2016. SMAP Level 3 Enhanced SM (cm^3/cm^3) for (c) February 1, 2016 and (d) July 10, 2016. Triangle and circle markers indicate the irrigated and non-irrigated sites, respectively.

An irrigated and a non-irrigated site (Fig. 2) are chosen for further analysis of temporal characteristics. Figure 3 shows SMAP SM at each of these sites (left axis), along with daily precipitation (right axis) from the Biggs CIMIS site. At both sites, SM is high November through March (i.e., 0.3 to 0.45 cm3/cm3), then gradually decreases from mid-March into April with the transition to the dry season. The sites behave similarly as they respond to widespread precipitation during the wet season. However, the sites abruptly diverge in May, exhibiting markedly different behavior for the rest of the growing season. The non-irrigated site dries down through May, responding to a few, small rainfall events. In contrast, SM at the irrigated site increases dramatically in May reaching and sustaining saturation from mid-May to mid-June. The timing is consistent with the USDA NASS crop reports that show planting of rice, which includes flood irrigation, in late April through May. During this time, the SM signal is in direct opposition to the rainfall (i.e., decreasing intensity, frequency), suggesting that the SM signal is in fact responding to the onset of flood irrigation.

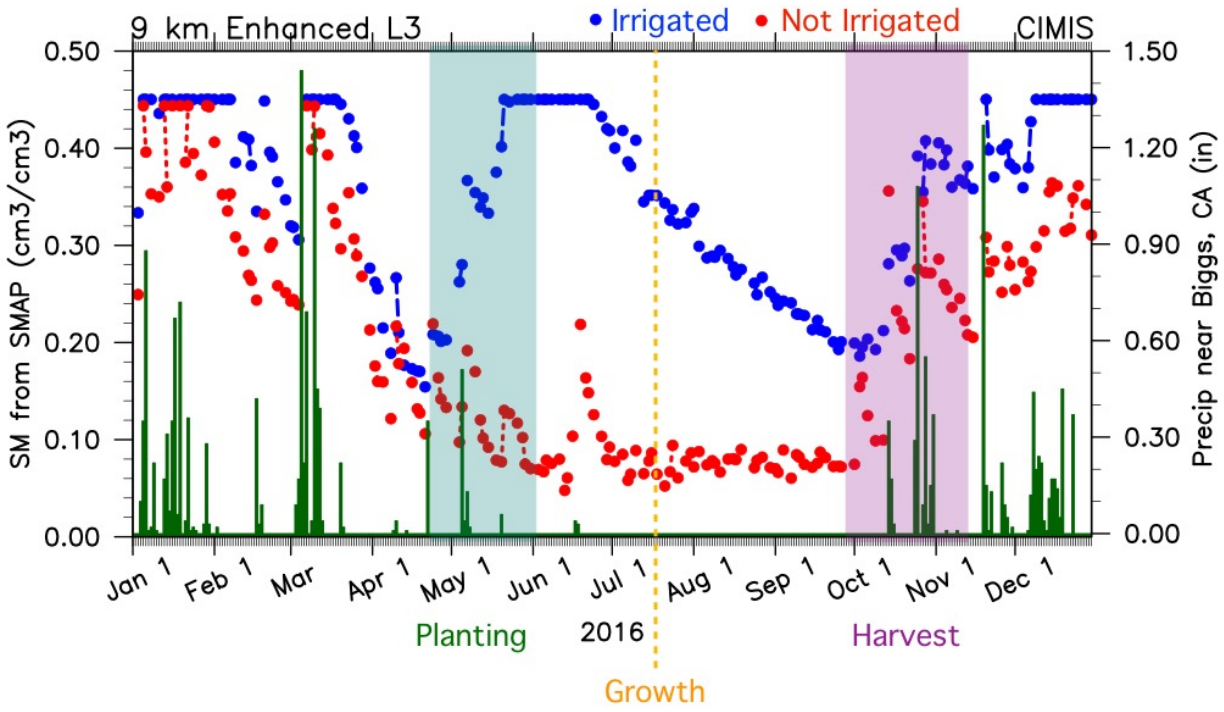

Figure 3. SMAP SM at the irrigated site (blue) as compared to the non-irrigated site (red) in the CCV. Right axis shows daily precipitation from the Biggs CIMIS site. Planting, growth, and harvest windows are from USDA NASS reports.

Beginning late in June, SM at the irrigated site steadily decreases until rain returns in October. The SMAP-sensed dry-down is likely a result of two factors. First, the crop report notes that in early July the rice has begun to "break out" of the water (i.e., "growth" in Fig. 3). This means the landscape SMAP senses has transitioned from essentially open water to water underneath vegetation, which increasingly attenuates the moisture signal with growth. Second, late in the summer the fields are drained before crop maturity and fall harvest (CA Rice, 2017). The harvest and growth periods are thus consistent with what is seen in the gradual decline of SMAP SM over the summer period.

Figure 4 shows the integrated SM and rainfall metric maps. As in the 14 July SM retrievals, the irrigated valley stands out as one of the wettest locations in the region, on par with the bordering mountains east of the Valley. The integrated rainfall shows that the precipitation falls along the higher elevations, wrapping around the valley. The irrigated valley is one of the wettest spots in the region in terms of SM, despite relatively little rainfall. Collectively, these analyses demonstrate that SMAP is able to identify the spatial signature and seasonal timing of irrigation in the Sacramento Valley.

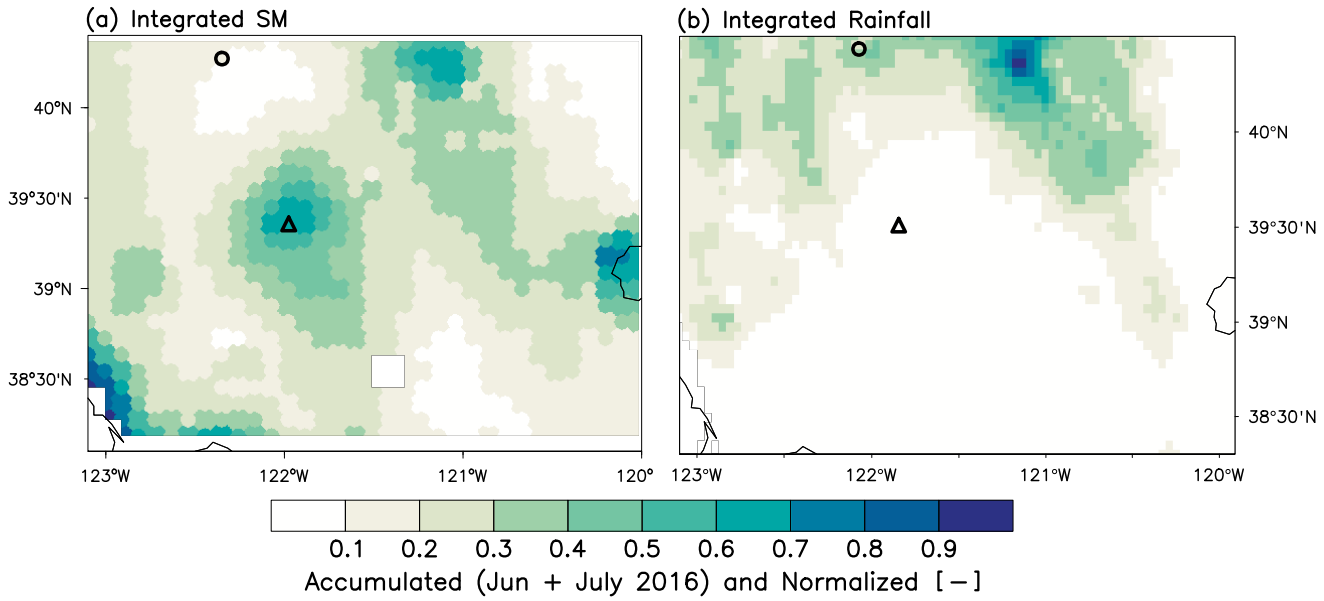

Figure 4. Time-integrated (June 1 to July 31) and normalized (a) SM and (b) precipitation. Markers as in Fig. 2.

3.2 San Luis Valley

The San Luis Valley (SLV) sits at an elevation over 2300 meters, nestled in between the San Juan and Sangre de Cristo mountains. Snow melt is the main source of irrigation water, through both surface water and aquifer recharge. Irrigation is clustered on the western side of the valley, where center pivot sprinklers irrigate predominately potatoes, alfalfa, and barley (USDA, 2017).

Figure 5b shows SMAP SM on 14 July 2016, masked out for all locations except the valley. The magnitude of SM is low, but the irrigated region stands out as being wetter (i.e., 0.025 cm^3/cm^3) than the surrounding area. This includes two local SM maxima apparent only during the growing season (S2). As in the CCV, the precipitation is confined mostly to the ridge tops and the integrated metrics show relatively high SM in June and July in the irrigated valley, despite little rainfall (Fig. 5c,d). This suggests that the relative SM and precipitation metric supports and is consistent with the onset and spatial extent of irrigation in this region.

It should be noted that the time series analyses of irrigated and non-irrigated areas (S2) are not as clear as in the CCV. A shift in trend is evident, whereby the irrigated area is often wetter in the growing season and the reverse is true in the off-season. However, these differences are small and within the range of instrument error (0.04 cm^3/cm^3), limiting robust conclusions from the time series analysis alone. These issues exhibit the difficulty of sensing a small area of irrigation closely bounded by complex topography.

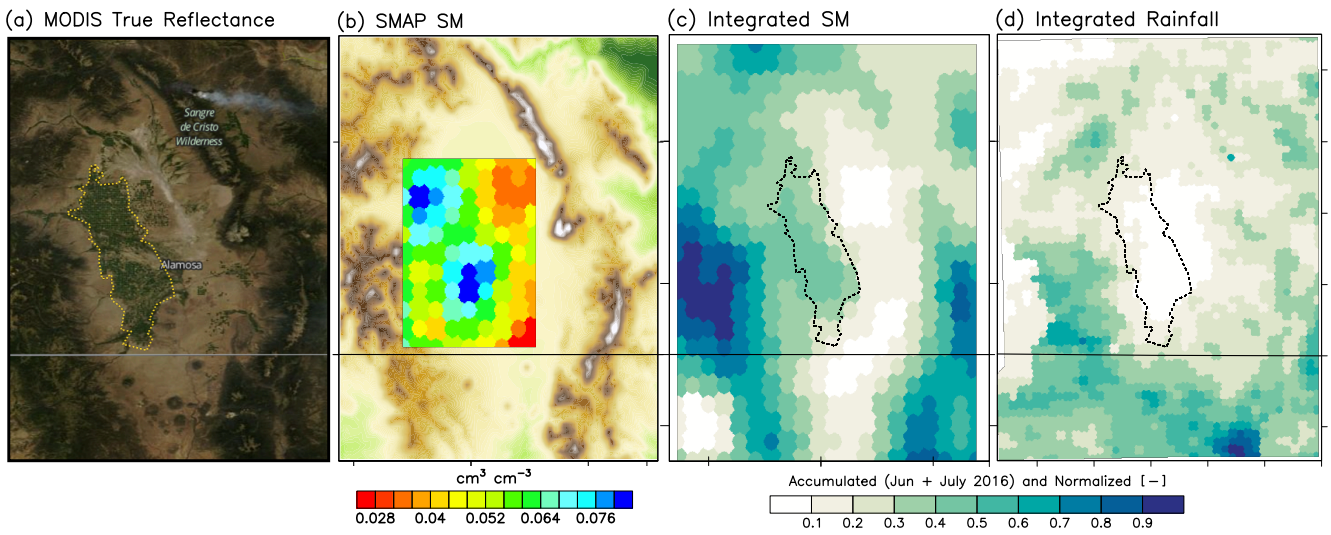

198

199 Figure 5. (a) MODIS Terra image of the SLV; irrigated valley outlined in yellow. (b) SMAP SM
200 retrievals on 14 July 2016 overlaid on a topography. Time-integrated and normalized (c) SM and
201 (d) rainfall; irrigated valley outlined in black.

202 3.3 Columbia River Valley

203 The third study region, referred to as the Columbia River Valley (CRV) for simplicity, is
204 actually centered on the convergence of three major rivers: the Columbia, the Snake, and the
205 Yakima. As these rivers are the primary source of irrigation water for eastern Washington, the
206 agriculture clings to the rivers and lowest elevations, creating a distinct pattern of greenness (Fig.
207 6a). In contrast to the other regions, a greater variety of crops are cultivated, including apples,
208 grapes, hops, among others (USDA, 2017). Drip irrigation has grown in popularity here, but
209 sprinkler and flood methods are still most common (USDA, 2013).

210 The spatial comparison of SM during and outside of the growing season, exhibits
211 elevated SM in July in areas of irrigation as compared to February, indicating that the irrigation
212 timing is again captured spatially (S3). Figure 6 (c, d), shows the integrated SM and rainfall
213 maps. As in the previous cases, rainfall is generally confined to the higher elevations creating a
214 rain-shadow and precipitation minimum for the valley in June and July. However, the integrated
215 SM shows elevated SM in the locations of the irrigated agriculture. Even more convincingly, the
216 shape of the elevated SM resembles the geography of the agriculture.

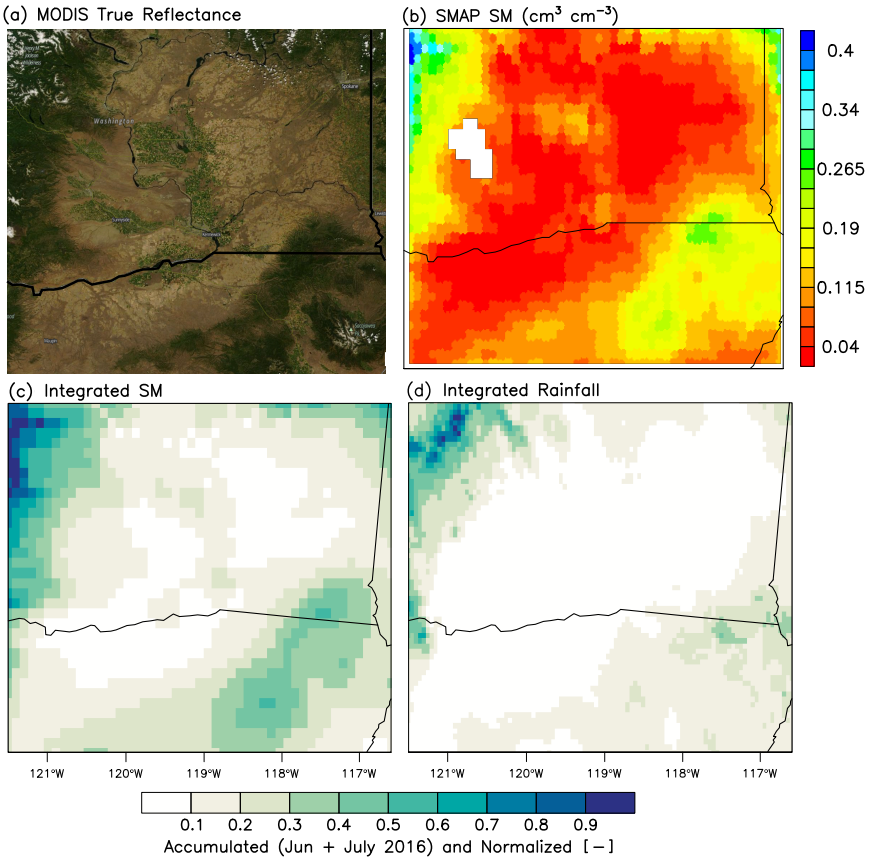

Figure 6. (a) Terra image of the CRV. (b) SMAP SM for 15 July 2016. Time-integrated and normalized (c) SM and (d) rainfall.

A complicating factor in this region is the irrigation's proximity to the large river systems and several lakes. Water bodies within the SMAP field of view could contaminate (i.e. incorrectly increase) the land SM near the rivers. This proves problematic, not only in the spatial plots, but also in defining appropriate locations for the time series analysis (S3). As in the SLV, there is a shift evident between the growing and off-season, but it is unclear to what extent the nearby water bodies, rather than the irrigated agriculture alone, contribute to this difference.

4 Discussion

The CCV was an ideal region for irrigation detection due to the consistent, extensive flood irrigation, ancillary observations, and rain-free summer. Flood irrigation proved the easiest method to detect, while comparatively water-conservative sprinkler irrigation in the SLV and CRV created subtler SM contrasts. The size of the irrigated area is also factor in detection. Although a 36x36km uniformly irrigated region could theoretically be captured by a perfectly aligned overpass, the likelihood of SMAP responding primarily to irrigation increases with the size of the irrigated area. The scale of irrigation at SLV is likely close to a practical minimum

required for SMAP-based detection based on these methods and results. In all three case studies, despite differences in irrigation scale and methods, the bulk, seasonal timing of irrigation was apparent in the spatial plots and integrated metrics.

The semi-arid, Mediterranean climate in these regions necessitates irrigation and creates the contrast between the irrigated and surrounding land. The same methods were applied to eastern Nebraska, where sprinkler irrigation is abundant but mainly used to increase yield, as precipitation is sufficient for rainfed crops. This means that satellite detection requires the identification of subtle differences between irrigated and rainfed SM. Not surprisingly, this proved a challenge for SMAP as no significant differences were found using the methods presented here.

A distinct advantage of microwave detection is that the most direct and observable impact of irrigation is in near-surface SM, the main product from SMAP, in contrast to optical/thermal detection that infers irrigation from surface temperature or other proxies. SMAP and thermal/optical-based products, such as high-resolution, area and time-limited irrigation mapping (e.g., Ozdogan and Gutman, 2008; Ambika et al., 2016) can be used together to evaluate and further develop irrigation physics, triggers, and thresholds in land surface models. SMAP-based detection also creates the possibility of incorporating the irrigation signal into models via DA systems to potentially improve forecasts.

As the SMAP record length grows, so too will the ability to mine these data to better understand human impacts on the water cycle. For example, if water conservation methods are widely adopted, how does the SM signal respond? SMAP-based irrigation detection can also be combined with groundwater observations to assist in monitoring agricultural water withdrawals and consumption.

5 Conclusions

This study demonstrated that in three semi-arid regions, SMAP is able to detect the bulk seasonal timing and spatial signature of irrigation via elevated SM relative to non-irrigated adjacent regions. Flood irrigation in the CCV yielded the most dramatic signature and showed SM dynamics consistent with local irrigation practices. In the other two regions, sprinkler irrigation resulted in subtler SM impacts that were often within the range of instrument error, prohibiting the type of intra-seasonal SM analysis that was completed in the CCV. Overall, these results indicate the potential for SMAP, future SM satellite missions, and enhanced products to be used for identifying the timing and location of irrigation. This potential will be more readily achieved with advances in resolution and retrieval over agricultural areas.

Acknowledgments, Samples, and Data

The authors declare no conflicts of interest. This work was supported by NASA grant NNH15ZDA001N-SUSMAP. SMAP data are available via: https://nsidc.org/data/smap/smap-data.html.

References

Alter, R. E., Im, E.-S., & Eltahir, E. A. B. (2015). Rainfall consistently enhanced around the Gezira Scheme in East Africa due to irrigation. *Nat. Geosci*, *8*(10), 763–767. doi:10.1038/ngeo2514.

Ambika, A. K., Wardlow, B., & Mishra, V. (2016). Remotely sensed high resolution irrigated area mapping in India for 2000 to 2015. *Sci. Data*, *3*, 160118. doi:10.1038/sdata.2016.118.

Bonfils, C. & Lobell, D. (2007). Empirical evidence for a recent slowdown in irrigation-induced cooling. *Proc. Natl. Acad. Sci*., *104*(34), 13582–7. doi:10.1073/pnas.0700144104.

California Rice (2017). How rice grows. California Rice Commission. Retrieved from http://calrice.org/pdf/How_Rice_Grows_final.pdf.

Colliander, A., et al. (2017). Validation of SMAP surface soil moisture products with core validation sites, *Remote Sens. Environ., 191,* 214-231. doi:10.1016/j.rse.2017.01.021.

Entekhabi, D. et al. (2010). The Soil Moisture Active Passive (SMAP) Mission. *Proc. IEEE*, *98*, 704-716. doi:10.1109/JPROC.2010.2043918

Evans, J. P. & Zaitchik, B. F. (2008). Modeling the large-scale water balance impact of different irrigation systems. *Water Resour. Res*., 44, W08448. doi:10.1029/2007WR006671.

Kanamaru, H. & Kanamitsu, M. (2008). Model diagnosis of nighttime minimum temperature warming during summer due to irrigation in the California Central Valley. *J. Hydrometeorol*., *9*(5), 1061–1072. doi:10.1175/2008JHM967.1.

Kumar, S. V., Peters-Lidard, C. D., Santanello, J. A., Reichle, R. H., Draper, C. S., Koster, R. D., Nearing, G. & Jasinski, M. F. (2015). Evaluating the utility of satellite soil moisture retrievals over irrigated areas and the ability of land data assimilation methods to correct for unmodeled processes. *Hydrol. Earth Syst. Sci*., *19*(11), 4463–4478. doi:10.5194/hess-19-4463-27015.

Kumar, S. V., Dirmeyer, P. A., Peters-Lidard, C. D., Bindlish, R., & Bolten, J. (2017). Information theoretic evaluation of satellite soil moisture retrievals, *Remote Sens. Environ*., (in press). doi:10.1016/j.rse.2017.10.016.

Kueppers, L. M., & Snyder, M. (2011). Influence of irrigated agriculture on diurnal surface energy and water fluxes, surface climate, and atmospheric circulation in California. *Clim. Dyn.*, *38* (5-6), 1017-1029. doi:10.1007/s00382-011-1123-0.

Lawston, P. M., Santanello, J. A., Zaitchik, B. F., & Rodell, M. (2015). Impact of irrigation methods on land surface model spinup and initialization of WRF forecasts. *J. Hydrometeorol., 16* (3), 1135–1154. doi:10.1175/JHM-D-14-0203.1.

Lawston, P.M., Santanello, J. A., Franz, T. E., & Rodell, M. (2017). Assessment of irrigation physics in a land surface modelling framework using non-traditional and human-practice datasets. *Hydrol. Earth Syst. Sci*., *21*, 2953-2966. doi:10.5194/hess-21-2953-2017.

Leng, G., Huang, M., Tang, Q., Gao, H., Leung, & L. R. (2014). Modeling the effects of groundwater-fed irrigation on terrestrial hydrology over the conterminous United States. *J. Hydrometeorol*., *15,* 957–972. doi:10.1175/JHM-D-13-049.1.

McColl, K. A., Wang, W., Peng, B., Akbar, R., Short Gianotti, D. J., Lu, H., Pan, M., & Entekhabi, D. (2017), Global characterization of surface soil moisture drydowns, *Geophys. Res. Lett., 44*, 3682–3690, doi:10.1002/2017GL072819.

O'Neill, P. E., Chan, S., Njoku, E. G., Jackson, T., & R. Bindlish, R. (2016). SMAP Enhanced L3 Radiometer Global Daily 9 km EASE-Grid Soil Moisture, Version 1. SPL3SMP_E.001. Boulder, Colorado USA. NASA National Snow and Ice Data Center Distributed Active Archive Center. doi: 10.5067/ZRO7EXJ8O3XI. March 20, 2017.

Ozdogan, M., and Gutman, G. (2008). A new methodology to map irrigated areas using multi-temporal MODIS and ancillary data: An application example in the continental U.S., *Remote Sens. Environ.,112*,3520-3537. doi:10.1016/j.rse.2008.04.010.

Ozdogan, M., Rodell, M., Beaudoing, H. K., & Toll, D. L. (2010). Simulating the effects of irrigation over the United States in a land surface model based on satellite derived agricultural data, *J. Hydrometeorol., 11*, 171–184. doi: 10.1175/2009JHM1116.1.

Pokhrel, Y. N., Hanasaki, N., Wada, Y., Kim, H. (2016). Recent progresses in incorporating human land-water management into global land surface models toward their integration into Earth system models. *Wiley Interdisciplinary Reviews: Water*, *3*(4), 548-574.

Puma, M. J. & Cook, B. I. (2010). Effects of irrigation on global climate during the 20th century. *J. Geophys. Res*., *115*, D16120. doi:10.1029/2010JD014122.

Qian, Y., Huang, M., Yang, B. & Berg, L. K. (2013). A modeling study of irrigation effects on surface fluxes and land–air–cloud interactions in the southern Great Plains. *J. Hydrometeorol*., *14*(3), 700–721. doi:10.1175/JHM-D-12-0134.1.

Salmon, J. M., Friedl, M. A., Frolking, S., Wisser, D., & Douglas, E. M. (2015). Global rain-fed, irrigated, and paddy croplands: A new high resolution map derived from remote sensing, crop inventories and climate data. *Int. J. Appl. Earth Obs. Geoinf*., *38*, 321–334. https://doi.org/10.1016/j.jag.2015.01.014.

Shellito, P. J., Small, E. E., Colliander, A., Bindlish, R., Cosh, M. H., Berg, A. A., Bosch, D. D., Caldwell, T. G., Goodrich, D. C., McNairn, H., Prueger, J. H., Starks, P. J., van der Velde, R., Walker, & J. P. (2016). SMAP soil moisture drying more rapid than observed in situ following rainfall events, *Geophys. Res. Lett.,43*(15). 43, 8068–8075, doi:10.1002/2016GL069946.

Sorooshian, S., Li, J., Hsu, K. & Gao, X. (2011). How significant is the impact of irrigation on the local hydroclimate in California's Central Valley? Comparison of model results with ground and remote-sensing data. *J. Geophys. Res*., *116*(D6), D06102. doi:10.1029/2010JD014775.

Thenkabail, P. S., Biradar, C. M., Noojipady, P., Dheeravath, V., Li, Y., Velpuri, M., Gumma, M., Gangalakunta, O., Turrai, H., Cai, X., Vithanage, J., Schull, M. A., Dutta, R. (2009). Global irrigated area map (GIAM), derived from remote sensing, for the end of the last millennium. *Internat. J. Remote Sens*., *30*(14), 3679-3733. doi:10.1080/01431160802698919.

USDA National Agricultural Statistics Service Cropland Data Layer (2017). Published crop-specific data layer [Online]. Accessed May 1 2017. USDA-NASS, Washington, DC, available at https://nassgeodata.gmu.edu/CropScape/.

USDA National Agricultural Statistics Service (2016). *California Crop Weather*. Retrieved from USDA NASS Pacific Field Office. Retrieved from https://www.nass.usda.gov/Statistics_by_State/California/Publications/Crop_Progress_&_Condition/